Evidence for topological band inversion of the phase change material Ge2Sb2Te5

Christian Pauly, Marcus Liebmann, Alessandro Giussani, Jens Kellner, Sven Just, Jaime Sánchez-Barriga, Emile Rienks, Oliver Rader, Raffaella Calarco, Gustav Bihlmayer, and Markus Morgenstern

Citation: Applied Physics Letters **103**, 243109 (2013); doi: 10.1063/1.4847715
View online: http://dx.doi.org/10.1063/1.4847715
View Table of Contents: http://scitation.aip.org/content/aip/journal/apl/103/24?ver=pdfcov
Published by the AIP Publishing

Evidence for topological band inversion of the phase change material $Ge_2Sb_2Te_5$

Christian Pauly,[1] Marcus Liebmann,[1] Alessandro Giussani,[2] Jens Kellner,[1] Sven Just,[1] Jaime Sánchez-Barriga,[3] Emile Rienks,[3] Oliver Rader,[3] Raffaella Calarco,[2] Gustav Bihlmayer,[4] and Markus Morgenstern[1]
[1]*II. Inst. Phys. B and JARA-FIT, RWTH Aachen University, 52074 Aachen, Germany*
[2]*Paul-Drude-Institut für Festkörperelektronik, Hausvogteiplatz 5-7, 10117 Berlin, Germany*
[3]*Helmholtz-Zentrum für Materialien und Energie, Elektronenspeicherring BESSY II, Albert-Einstein-Strasse 15, 12489 Berlin, Germany*
[4]*Peter Grünberg Institut (PGI-1) and Institute for Advanced Simulation (IAS-1), Forschungszentrum Jülich and JARA, 52425 Jülich, Germany*

(Received 29 August 2013; accepted 25 November 2013; published online 11 December 2013)

We present an angle-resolved photoemission study of a ternary phase change material, namely $Ge_2Sb_2Te_5$, epitaxially grown on Si(111) in the metastable cubic phase. The observed upper bulk valence band shows a minimum at $\bar{\Gamma}$ being 0.3 eV below the Fermi level E_F and a circular Fermi contour around $\bar{\Gamma}$ with a dispersing diameter of 0.27–0.36 $Å^{-1}$. This is in agreement with density functional theory calculations of the Petrov stacking sequence in the cubic phase which exhibits a topological surface state. The topologically trivial cubic Kooi-De Hosson stacking shows a valence band maximum at Γ in line with all previous calculations of the hexagonal stable phase exhibiting the valence band maximum at Γ for a trivial $\mathbb{Z}_2$ topological invariant ν_0 and away from Γ for non-trivial ν_0. Scanning tunneling spectroscopy exhibits a band gap of 0.4 eV around E_F.
 [http://dx.doi.org/10.1063/1.4847715]

Following the proposal[1,2] and discovery[3,4] of topological insulators (TIs), materials are currently optimized in terms of separating the Dirac cone from bulk bands and tuning the Dirac point close to the Fermi energy E_F. In this course, compounds involving more than two elements are preferentially used since they offer more degrees of freedom.[5,6] Connecting such compounds to classes of materials already in use for electronic or storage applications is desirable towards the utilization of topological properties. An important material system for commercially used optical and non-volatile electrical data storage is phase change materials (PCMs),[7,8] which are found predominantly along the pseudobinary line connecting GeTe and Sb_2Te_3.[9]

Such PCMs exhibit a large contrast in electronic and optical properties upon changing from amorphous to crystalline.[10,11] Using laser-induced or electrical heat pulses, the switching occurs within nanoseconds[12] or below[13] at an energy cost of only 1 fJ.[14] The PCM Sb_2Te_3 is experimentally known to be a TI[15–17] and some of the other compounds on the pseudobinary line are predicted to be TIs based on density functional theory (DFT) calculations.[5,18–21] $Ge_2Sb_2Te_5$ (GST-225) is at the borderline of these predictions,[19,21] i.e., its TI properties depend on the stacking sequence.[21] Here, we present experimental evidence for the non-trivial topology of GST-225 by angle-resolved photoemission spectroscopy (ARPES), supported by DFT calculations. The result implies that half of the pseudobinary line consists of TIs and opens up the perspective for fast and reversible switching between a crystalline topological phase and an insulating amorphous phase.

GST-225, a prototype PCM, emerges in two slightly different crystalline phases, a metastable cubic one used for applications[22] and a stable hexagonal one. Within the stable phase, hexagonal layers are stacked along [0001] with a sequence deduced from transmission electron microscopy (TEM) to be either Te-Sb-Te-Ge-Te-v-Te-Ge-Te-Sb- (Petrov phase)[23] or Te-Ge-Te-Sb-Te-v-Te-Sb-Te-Ge- (Kooi-De Hosson or KH phase).[24] The v denotes a vacancy layer, where adjacent Te layers are van-der-Waals bonded. DFT calculations imply that the KH phase is energetically favorable.[25] More recent X-ray diffraction data suggest some mixture of Ge and Sb in the respective layers.[26] The cubic rocksalt structure exhibits hexagonal layers stacked along [111] with $(Te–Ge/Sb/v)_3$ sequence, where Ge/Sb/v is a mixed layer of Ge, Sb, and vacancies.[26,27] More recent TEM studies suggest that the Ge/Sb/v layers exhibit some internal order[28] and DFT even implies that Ge, Sb, and vacancies accumulate in separate layers.[25] Thus, the stable and the metastable phase could be much closer than originally anticipated. Then, the transition between them would be a mere shift of blocks of (111) layers without atomic rearrangements within the layers.[25]

The first prediction of topologically insulating GST-225 was made by Kim *et al.* for the Petrov phase while the energetically favorable KH phase was shown to be topologically trivial.[18] However, even the KH phase of GST-225 can be made a TI by DFT if set under isotropic pressure[29] or strain.[30] A more disordered, hexagonal mixed-layer phase was investigated by Silkin *et al.* by DFT with the stacking sequence Te-M1-Te-M2-Te-v-Te-M2-Te-M1- having $Ge_{2x}Sb_{2(1-x)}$ in M1 and $Ge_{2(1-x)}Sb_{2x}$ in M2.[21] The transition between the Petrov ($x = 0$) and the KH ($x = 1$) phase exhibits a semimetal for the Petrov phase, a trivial band insulator for $x = 1$ and $x = 0.75$, and a topological insulator for $x = 0.25$ and $x = 0.5$.

Importantly, all DFT calculations of GST-225 exhibiting the valence band maximum (VBM) away from Γ show topologically non-trivial properties.[18,19,21,29,30] The only exception is the Petrov phase calculated by Silkin *et al.* which is

semimetallic.[21] This empirical relation is our central argument in the following.

So far, there have been no calculations including spin-orbit coupling for the metastable rocksalt phase. We will provide them for the Petrov and KH stacking, confirming the above trend. To ease the comparison of our data also with previous calculations, we stick to the hexagonal nomenclature also for the metastable cubic phase, identifying the cubic [111] with the hexagonal [0001] direction.

In order to study TI properties by ARPES, ideally single crystalline GST is desired. Typically, GST is deposited in a polycrystalline fashion by physical vapor deposition. Only recently, epitaxial films of superior crystalline quality have been grown molecular beam epitaxy (MBE) on GaSb, InAs, and Si.[31–35] The metastable cubic, rhombohedrally distorted GST-225 grows with a single vertical epitaxial orientation, well defined interfaces, and atomically flat terraces only on (111)-oriented substrates.[31,32]

The GST-225 layers were grown on Si(111) in an MBE machine dedicated to chalcogenides.[36] The temperature of the effusion cells was set such that the flux ratio of Ge:Sb:Te is close to 2:2:5, as confirmed by X-ray fluorescence.[31,32] Out-of-plane and grazing incidence X-ray diffraction (XRD) shows that GST grows in the metastable cubic phase along the [111] direction. The presence of superstructure peaks in addition to the Bragg reflections of cubic GST-225 indicates vacancy ordering in the Ge/Sb/v sublattice along the growth direction. The film thickness was 20 nm, and the growth temperature was 250 °C.

After growth, the samples have been transferred under ambient conditions. Before insertion into the ultrahigh vacuum ARPES or scanning tunneling microscopy (STM) chambers, the surface was deoxidized by dipping in deionized (DI) water for 1 min following the procedure of Zhang *et al.*[37] Afterwards, the sample was introduced within 2 min and, after pump-down, annealed to 250 °C yielding a clean crystalline, stoichiometric, and oxygen-free surface.[36] XRD data confirm that neither this procedure nor the subsequent measurements change the phase of the GST-225.

The topography was investigated by atomic force microscopy (AFM) on a μm scale and by STM on the nm scale. The AFM topography (Fig. 1(a)) exhibits an overall roughness of 3–4 nm_{rms} due to pyramids with 5–15 nm in height and a width close to 1 μm. On their slopes, atomically flat terraces up to 100 nm in width are found (Fig. 1(c)). These terraces are separated by steps of 0.34 ± 0.01 nm in height, in agreement with the expected Te-Te layer distance of 0.347 nm in cubic GST-225.[38] On the terraces, atomic resolution is achieved by STM (Fig. 1(d)), most likely showing the Te layer.[39] Scanning tunneling spectroscopy (STS) shows a band gap of 0.4 eV with E_F situated at the top of the valence band (Fig. 1(b)).

ARPES measurements have been performed at the beamline UE112-lowE-PGM2 (1^2) at BESSY II using a Scienta R8000 analyzer. Figure 2(a) displays a spectrum recorded with linearly polarized light at $h\nu = 22$ eV in a direction determined to be $\bar{\Gamma} - \bar{K}$ by comparison with DFT calculations.[36] Just below E_F, the upper valence band shows maxima at $k_{\|} = \pm 0.14 \pm 0.02$ Å^{-1} and drops to $E - E_F = -0.3$ eV at $\bar{\Gamma}$. Another band resides between -0.7 eV at $k_{\|} = \pm 0.23$ Å^{-1}

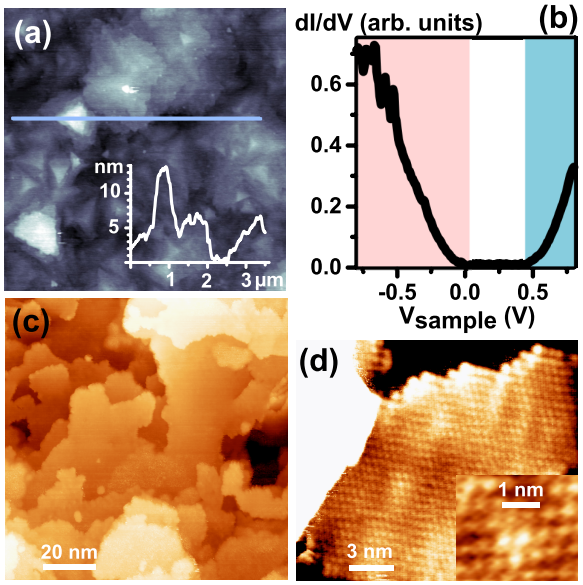

FIG. 1. Scanning probe microscopy of metastable GST-225 (111) after DI water dip. (a) Tapping mode AFM under ambient conditions. Inset: profile along the line marked in the image. (b) STS curve recorded in UHV (average of 10 spectra). Red/light shaded (blue/darker) area marks the valence (conduction) band. Stabilization at $V_{sample} = -0.8$ V, $I = 100$ pA. (c) STM image of atomically flat terraces. Average step height: 0.34 nm. $V_{sample} = -0.3$ V, $I = 100$ pA. (d) STM image with atomic resolution (inset: zoom). $V_{sample} = -0.5$ V, $I = 100$ pA. All data are taken at room temperature.

and -0.35 eV at $k_{\|} = \pm 0.1$ Å^{-1}. Closer to $\bar{\Gamma}$, these two bands lead to a broad peak in energy distribution curves (EDCs) around -0.4 eV with a FWHM of 0.5 eV (Fig. 3(a)). Below -1 eV, there are two more hole-like bands. The $\bar{\Gamma} - \bar{M}$ direction looks essentially the same with slightly more intensity at even higher $|k|$ values.[36] This can be seen from the constant energy cut at E_F in Fig. 2(b), showing a nearly isotropic circle and faint additional intensity at high $|k|$ values in the six different $\bar{\Gamma} - \bar{M}$ directions.

DFT calculations have been performed within in the generalized gradient approximation.[40] We employed the full-potential linearized augmented planewave method in bulk and thin-film geometry[41] as implemented in the FLEUR

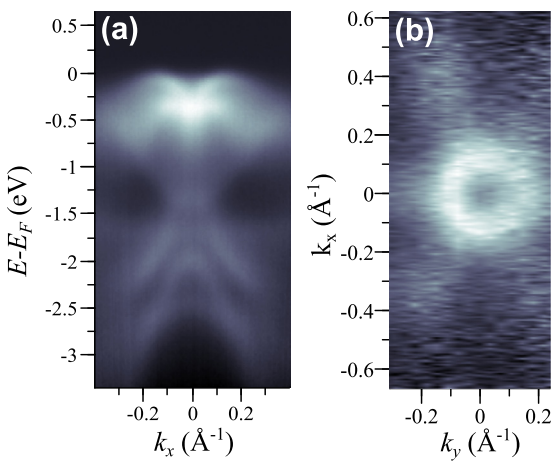

FIG. 2. ARPES spectra of metastable GST-225 (111) after DI water dip: (a) recorded in $\bar{\Gamma} - \bar{K}$ direction (see Ref. 36, Shirley-type background subtracted), (b) intensity in the $k_{\|}$ plane at E_F, $\bar{\Gamma} - \bar{M}$ direction is horizontal; photon energy: 22 eV, temperature: 300 K.

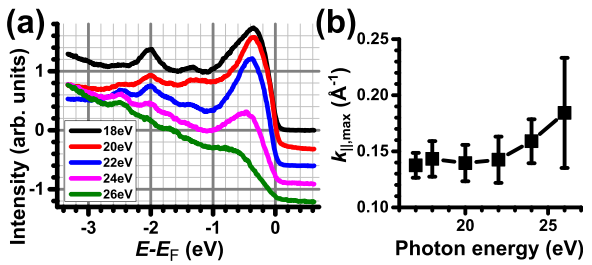

FIG. 3. Effects of photon energy variation. (a) EDCs at $\bar{\Gamma}$ for photon energies $h\nu = 18 - 26\,\text{eV}$ (top-down) as indicated, corresponding to a k_z variation of $\Delta k_z \approx 0.35\,\text{Å}^{-1}$. Graphs are offset for clarity. (b) $k_\parallel$-value of the valence band maximum ($\bar{\Gamma} - \bar{K}$ direction) as extracted from spectra at different photon energies.

code.[36] Spin-orbit coupling was included self-consistently, and a basis set cutoff of $R_{\text{MT}}\, k_{\text{max}} = 9$ was used. As structural model for the cubic phases we adopted the atomic positions given by Sun *et al.*,[25] both for the bulk and film structures. For the latter, films consisting of 27 atomic layers terminating by a "vacancy layer" were used. Two different stacking sequences were assumed for the cubic phase: a Petrov- and a KH-like sequence, which are derived from the respective hexagonal phases by tripling the unit cell and adding appropriate shifts.

Figure 4 shows the 2nd derivative of the measured band structure along with the calculations. A reasonable agreement is only achieved with the Petrov-like stacking, including the minimum at $\bar{\Gamma}$ of the upper valence band. The bands further down in energy (around $-0.6\,\text{eV}$ at $\bar{\Gamma}$) can be associated with a Rashba-type surface state, similar to the one observed in Sb_2Te_3.[17] In close vicinity of the upper valence band, the calculation shows the topological surface state crossing the Fermi energy at $k_\parallel \approx 0.12\,\text{Å}^{-1}$. This state obviously overlaps with the upper bulk valence band within our ARPES data.

In order to probe different k_z and, thus, distinguish surface from bulk states, spectra with $h\nu = 17 - 26\,\text{eV}$ have been recorded.[36] Corresponding EDCs at $\bar{\Gamma}$ are shown in Fig. 3(a). The topmost maximum shifts down by about 0.2 eV between $h\nu = 22\,\text{eV}$ and 26 eV, indicating a k_z dispersion, as expected for a band with bulk character. The $k_\parallel$-position of the VBM has been evaluated by means of the 2nd derivative of the ARPES spectra: the EDC with the peak at the highest energy is chosen, and the corresponding $k_\parallel$ value is taken as $k_{\parallel,\text{max}}$.[36] Figure 3(b) displays $k_{\parallel,\text{max}}$ as a function of photon energy revealing a small dependence on k_z as well. Thus, the ARPES peak at the VBM is, at least partially, a bulk band with dispersion in k_z direction.

The calculated $k_{\parallel,\text{max}}$ of the bulk valence band (0.19–0.22 Å^{-1}) is larger than the experimental one (0.14–0.18 Å^{-1}). This can be explained by the overlap with the surface state which crosses E_F at $k_\parallel \approx 0.12\,\text{Å}^{-1}$ (Fig. 4). The small anisotropy of $k_{\parallel,\text{max}}$ (DFT: 7%, ARPES: <10%) between $\bar{\Gamma} - \bar{M}$ and $\bar{\Gamma} - \bar{K}$ was not detectable within the experimental error.

We finally compare the metastable cubic phase with previous DFT calculations of the very similar hexagonal phase. Most notably, a VBM away from $\bar{\Gamma}$ consistently indicates topologically non-trivial properties for GST-225.[18,19,21,29,30] Albeit such a relation is also found for the 3D TIs BiSb,[4,42] Bi_2Te_3,[16,43] and Sb_2Te_3,[15–17] it is currently under discussion for Bi_2Se_3.[16,44,45] None of these materials have a VBM away from Γ with trivial properties.[46] The measured $k_{\parallel,\text{max}}$ is smaller than the calculated $k_{\parallel,\text{max}}$ of the bulk VBM of topologically non-trivial hexagonal stable phases of GST-225 (0.16–0.52 Å^{-1}).[36] The superposition of bulk valence band and topological surface state in the ARPES data might be relevant again.

In summary, we have shown by ARPES and STS that metastable cubic $Ge_2Sb_2Te_5$ epitaxially grown on Si(111) exhibits valence band maxima 0.14–0.18 Å^{-1} away from $\bar{\Gamma}$ and a band gap of 0.4 eV. All DFT calculations of $Ge_2Sb_2Te_5$ find a VBM away from Γ only for a $\mathbb{Z}_2$ topological invariant $\nu_0 = 1$. This implies topological properties of $Ge_2Sb_2Te_5$, indicates that all phase change materials on the pseudobinary line between Sb_2Te_3 and $Ge_2Sb_2Te_5$ are topologically non-trivial, and opens up the possibility of switching between an insulating amorphous phase and a topological phase on ns time scales.

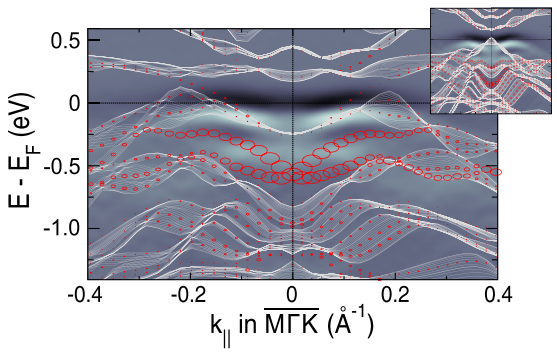

FIG. 4. DFT calculations of the band structures for cubic GST-225 with Petrov- and KH-type (inset, same scale as main image) stacking sequence, as proposed in Ref. 25. Bulk bands are given as gray lines, states of the film calculations with circles. The extension of the states into the vacuum (region above the topmost Te layer) is indicated by the size of the circles. The calculations are superimposed with the ARPES spectra (2nd derivative of intensity with respect to electron energy) at 22 eV photon energy. Calculations are shifted upwards by 100 meV.

We gratefully acknowledge financial support by the German Science Foundation (DFG): SFB 917, Project A3, the SPP 1666 "Topological Insulators" and Mo058/13-1; the Helmholtz-Zentrum Berlin (HZB); the excellence initiative of the German federal government; and the Fonds National de la Recherche (Luxembourg). We thank F. Lange, S. Behnke, and C. Stemmler for technical support.

[1]B. A. Volkov and O. A. Pankratov, JETP Lett. **42**, 178 (1985).
[2]L. Fu, C. L. Kane, and E. J. Mele, Phys. Rev. Lett. **98**, 106803 (2007).
[3]M. König, S. Wiedmann, C. Brüne, A. Roth, H. Buhmann, L. W. Molenkamp, X.-L. Qi, and S.-C. Zhang, Science **318**, 766 (2007).
[4]D. Hsieh, D. Qian, L. Wray, Y. Xia, Y. S. Hor, R. J. Cava, and M. Z. Hasan, Nature **452**, 970 (2008).
[5]S. V. Eremeev, G. Landolt, T. V. Menshchikova, B. Slomski, Y. M. Koroteev, Z. S. Aliev, M. B. Babanly, J. Henk, A. Ernst, L. Patthey *et al.*, Nat. Commun. **3**, 635 (2012).
[6]Y. Ando, J. Phys. Soc. Jpn. **82**, 102001 (2013).
[7]M. Wuttig and N. Yamada, Nature Mater. **6**, 824 (2007).
[8]M. Wuttig and S. Raoux, Z. Anorg. Allg. Chem. **638**, 2455 (2012).
[9]D. Lencer, M. Salinga, B. Grabowski, T. Hickel, J. Neugebauer, and M. Wuttig, Nature Mater. **7**, 972 (2008).
[10]S. R. Ovshinsky, Phys. Rev. Lett. **21**, 1450 (1968).

[11]N. Yamada, E. Ohno, N. Akahira, K. Nishiuchi, K. Nagata, and M. Takao, Jpn. J. Appl. Phys. **26**, 61 (1987).
[12]N. Yamada, E. Ohno, K. Nishiuchi, N. Akahira, and M. Takao, J. Appl. Phys. **69**, 2849 (1991).
[13]D. Loke, T. H. Lee, W. J. Wang, L. P. Shi, R. Zhao, Y. C. Yeo, T. C. Chong, and S. R. Elliott, Science **336**, 1566 (2012).
[14]F. Xiong, A. D. Liao, D. Estrada, and E. Pop, Science **332**, 568 (2011).
[15]D. Hsieh, Y. Xia, D. Qian, L. Wray, F. Meier, J. H. Dil, J. Osterwalder, L. Patthey, A. V. Fedorov, H. Lin *et al.*, Phys. Rev. Lett. **103**, 146401 (2009).
[16]H. Zhang, C.-X. Liu, X.-L. Qi, X. Dai, Z. Fang, and S.-C. Zhang, Nat. Phys. **5**, 438 (2009).
[17]C. Pauly, G. Bihlmayer, M. Liebmann, M. Grob, A. Georgi, D. Subramaniam, M. R. Scholz, J. Sanchez-Barriga, A. Varykhalov, S. Blügel *et al.*, Phys. Rev. B **86**, 235106 (2012).
[18]J. Kim, J. Kim, and S.-H. Jhi, Phys. Rev. B **82**, 201312 (2010).
[19]J. Kim, J. Kim, K.-S. Kim, and S.-H. Jhi, Phys. Rev. Lett. **109**, 146601 (2012).
[20]J. Kim and S.-H. Jhi, Phys. Status Solidi B **249**, 1874 (2012).
[21]I. V. Silkin, Y. M. Koroteev, G. Bihlmayer, and E. V. Chulkov, Appl. Surf. Sci. **267**, 169 (2013).
[22]J.-B. Park, G.-S. Park, H.-S. Baik, J.-H. Lee, H. Jeong, and K. Kim, J. Electrochem. Soc. **154**, H139 (2007).
[23]I. I. Petrov, R. M. Imamov, and Z. G. Pinsker, Sov. Phys. Crystallogr. **13**, 339 (1968).
[24]B. J. Kooi and J. T. M. D. Hosson, J. Appl. Phys. **92**, 3584 (2002).
[25]Z. Sun, J. Zhou, and R. Ahuja, Phys. Rev. Lett. **96**, 055507 (2006).
[26]T. Matsunaga, N. Yamada, and Y. Kubota, Acta Crystallogr. B **60**, 685 (2004).
[27]N. Yamada and T. Matsunaga, J. Appl. Phys. **88**, 7020 (2000).
[28]Y. J. Park, J. Y. Lee, M. S. Youm, Y. T. Kim, and H. S. Lee, J. Appl. Phys. **97**, 093506 (2005).
[29]B. Sa, J. Zhou, Z. Song, Z. Sun, and R. Ahuja, Phys. Rev. B **84**, 085130 (2011).
[30]B. Sa, J. Zhou, Z. Sun, and R. Ahuja, Europhys. Lett. **97**, 27003 (2012).
[31]F. Katmis, R. Calarco, K. Perumal, P. Rodenbach, A. Giussani, M. Hanke, A. Proessdorf, A. Trampert, F. Grosse, R. Shayduk *et al.*, Cryst. Growth Des. **11**, 4606 (2011).
[32]P. Rodenbach, R. Calarco, K. Perumal, F. Katmis, M. Hanke, A. Proessdorf, W. Braun, A. Giussani, A. Trampert, H. Riechert *et al.*, Phys. Status Solidi (RRL) **6**, 415 (2012).
[33]Y. Takagaki, A. Giussani, K. Perumal, R. Calarco, and K.-J. Friedland, Phys. Rev. B **86**, 125137 (2012).
[34]A. Giussani, K. Perumal, M. Hanke, P. Rodenbach, H. Riechert, and R. Calarco, Phys. Status Solidi B **249**, 1939 (2012).
[35]Y. Takagaki, A. Giussani, J. Tominaga, U. Jahn, and R. Calarco, J. Phys. Condens. Matter **25**, 345801 (2013).
[36]See supplementary material at http://dx.doi.org/10.1063/1.4847715 for further information on sample preparation, crystallographic directions, additional ARPES spectra, and calculations.
[37]Z. Zhang, J. Pan, Y. L. Foo, L. W.-W. Fang, Y.-C. Yeo, R. Zhao, L. Shi, and T.-C. Chong, Appl. Surf. Sci. **256**, 7696 (2010).
[38]T. Nonaka, G. Ohbayashi, Y. Toriumi, Y. Mori, and H. Hashimoto, Thin Solid Films **370**, 258 (2000).
[39]V. L. Deringer and R. Dronskowski, J. Phys. Chem. C **117**, 15075 (2013).
[40]J. P. Perdew, K. Burke, and M. Ernzerhof, Phys. Rev. Lett. **77**, 3865 (1996).
[41]H. Krakauer, M. Posternak, and A. J. Freeman, Phys. Rev. B **19**, 1706 (1979).
[42]D. Hsieh, Y. Xia, L. Wray, D. Qian, A. Pal, J. H. Dil, J. Osterwalder, F. Meier, G. Bihlmayer, C. L. Kane *et al.*, Science **323**, 919 (2009).
[43]D. Hsieh, Y. Xia, D. Qian, L. Wray, J. H. Dil, F. Meier, J. Osterwalder, L. Patthey, J. G. Checkelsky, N. P. Ong *et al.*, Nature **460**, 1101 (2009).
[44]Y. Xia, D. Qian, D. Hsieh, L. Wray, A. Pal, H. Lin, A. Bansil, D. Grauer, Y. S. Hor, R. J. Cava *et al.*, Nat. Phys. **5**, 398 (2009).
[45]I. A. Nechaev, R. C. Hatch, M. Bianchi, D. Guan, C. Friedrich, I. Aguilera, J. L. Mi, B. B. Iversen, S. Blügel, P. Hofmann *et al.*, Phys. Rev. B **87**, 121111 (2013).
[46]I. Aguilera, C. Friedrich, G. Bihlmayer, and S. Blügel, Phys. Rev. B **88**, 045206 (2013).